Frequency-dependent magneto-optical conductivity in the generalized α-T_3 model

Áron Dániel Kovács,[1] Gyula Dávid,[2] Balázs Dóra,[3] and József Cserti[1]

[1]*Department of Physics of Complex Systems, Eötvös University, H-1117 Budapest, Pázmány Péter sétány 1/A, Hungary*

[2]*Department of Atomic Physics, Eötvös University, H-1117 Budapest, Pázmány Péter sétány 1/A, Hungary*

[3]*Department of Theoretical Physics and BME-MTA Exotic Quantum Phases Research Group, Budapest University of Technology and Economics, Budapest, Hungary*

(Received 31 May 2016; revised manuscript received 12 September 2016; published 12 January 2017)

We have studied a generalized three-band crossing model in 2D, the generalized α-T_3 lattice, ranging from the pseudospin-1 Dirac equation through a quadratic+flat band touching to the pseudospin-1/2 Dirac equation. A general method is presented to determine the operator form of the Green's function, being gauge and representation independent. This yields the Landau level structure in a quantizing magnetic field and the longitudinal and transversal magneto-optical conductivities of the underlying system. Although the magneto-optical selection rules allow for many transitions between Landau levels, the dominant one stems from exciting a particle from/to the flat band to/from a propagating band. The Hall conductivity from each valley is rational (not quantized at all), in agreement with Berry phase considerations, though their sum is always integer quantized.

DOI: 10.1103/PhysRevB.95.035414

I. INTRODUCTION

Since the first isolation of graphene [1] in 2004 and the theoretical prediction and experimental realization of topological insulators [2,3], the Dirac equation and its variants have started to attract almost unprecedented attention in condensed matter and related fields. The peculiar spinor structure of the Dirac equation, which, e.g., stems from the two sublattices of the 2D honeycomb lattice in graphene, gives rise to many topology related phenomena such as a Berry phase [1] of π, unusual Landau quantization in a magnetic field and the related unconventional quantum Hall effect [4], just to mention a few immediate consequences.

The 2D massless Dirac equation possesses the deceivingly simple form as

$$H_{S=1/2} = v_F \mathbf{S}\cdot\mathbf{p} = v_F \begin{bmatrix} 0 & p_- \\ p_+ & 0 \end{bmatrix}, \tag{1}$$

where v_F is the Fermi velocity of the underlying system and plays the role of the effective speed of light, $\mathbf{p} = (p_x, p_y)$ is the 2D momentum, $p_\pm = p_x \pm i p_y$ and $\mathbf{S}$ stands for the spin-1/2 Pauli matrices, which represent the sublattice degree of freedom in this instance. Shortly after the discovery of graphene, this equation was generalized, still in 2D, to arbitrary pseudospin-S, known as the Dirac-Weyl equation with $\mathbf{S}$ now representing the $(2S+1)\times(2S+1)$ matrix representations of the $SU(2)$ algebra, and several lattices have been proposed, hosting these Weyl fermions [5–9].

Similarly to other spin-S problems, cases with integer and half-integer spin differ from each other. The ensuing spectrum consists of coaxial Dirac cones, crossing each other at the same Dirac point, and for integer spins, an additional dispersionless flat band also shows up and crosses the Dirac point.

The simplest integer spin case is the pseudospin-1 Weyl equation. It has a 3×3 matrix structure as

$$H_{S=1} = v_F \begin{bmatrix} 0 & p_- & 0 \\ p_+ & 0 & p_- \\ 0 & p_+ & 0 \end{bmatrix}, \tag{2}$$

and in comparison to Eq. (1), many more new terms can be added to this and masses can be opened in several distinct ways [10]. As detailed below, Eq. (2) can be realized in the dice or T_3 lattice, composed of two 2D honeycomb lattices, which share one sublattice and is sketched in Fig. 1. Experimentally, the dice lattice can be realized from a trilayer structure of the face-centred cubic lattice, grown in the [111] direction [10].

Recently, a novel variant of the T_3 lattice structure was proposed, coined as the α-T_3 model, suggested first by Raoux *et al.* [12]. Due to the three nonequivalent lattice sites of the T_3 lattice, two nearest-neighbor hopping integrals are possible, which, however, need not be equal to each other. The generalized α-T_3 model is described alternatively by a lattice consisting of three layers of triangular lattices with basis atoms A, B, and C and with only intersublattice hoppings between adjacent layers shown in Fig. 1. By tuning a parameter α, which measures the relative strength of the two hopping integrals, one can interpolate continuously from the $S = 1/2$ case with a completely decoupled flat band to the perfect $S = 1$ situation, i.e., from the physics of Eq. (1) to Eq. (2). The three-band tight-binding Hamiltonian in the basis A, B, and C is given by [7,10,13,14]

$$H_{\rm dice} = \begin{pmatrix} 0 & t_1 f(\boldsymbol{k}) & 0 \\ t_1 f^*(\boldsymbol{k}) & \epsilon_0 & t_2 f(\boldsymbol{k}) \\ 0 & t_2 f^*(\boldsymbol{k}) & 0 \end{pmatrix}, \tag{3}$$

where t_1 and t_2 are the hopping amplitudes between adjacent triangular lattice, and it has further been generalized by adding [11,14] an on-site energy term ϵ_0 in the middle layer, arising from, e.g., a real chemical potential, while $f(\boldsymbol{k}) = 1 + 2\exp(i3k_y a/2)\cos(\sqrt{3}k_x a/2)$ with $\boldsymbol{k} = (k_x, k_y)$ and a is the nearest-neighbor distance in the dice lattice (the distance between sites A and B), and $*$ denotes the complex conjugation. In the original formulation of the model, $t_2/t_1 = \tan(\phi) = \alpha$ was used for parametrization, but we prefer to use the two hopping amplitudes instead. Although the spectrum itself is independent from α, the Berry phase depends continuously on it.

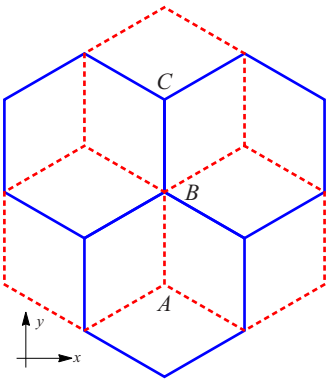

FIG. 1. The dice lattice with t_1 and t_2 hopping amplitude along the red dashed and blue solid lines. The on-site energy of the sixfold connected site B is ϵ_0. There are three atoms A, B, and C in each unit cell.

The ϵ_0 term changes the spectrum of the model, and results in a parabolic band touching a flat band, and an additional decoupled parabolic band, as sketched in Fig. 2. The touching parabolic and flat band realizes essentially the same physics as bilayer graphene, which possesses two touching parabola, as was emphasized in Ref. [14]. Then, tuning also the hopping integrals $t_{1,2}$, the strength of the coupling between the touching parabolic and flat band can be continuously tuned. In turn, this allows us to study single and bilayer graphene physics as well as the pseudospin-1 Dirac-Weyl equation within the same model.

Linearizing the function $f(\boldsymbol{k})$ around the $\mathbf{K} = (2\pi/3\sqrt{3}a, 2\pi/3a)$ point in the Brillouin zone we have $f(\boldsymbol{K}+\boldsymbol{k}) \approx (3a/2)(k_x - ik_y)$. Then, the linearized form of the Hamiltonian (3) for low-energy states (around the $\mathbf{K}$ point) reads

$$H_K = \frac{3a}{2}\begin{pmatrix} 0 & t_1 k_- & 0 \\ t_1 k_+ & \epsilon_0 & t_2 k_- \\ 0 & t_2 k_+ & 0 \end{pmatrix}, \tag{4}$$

where $k_\pm = k_x \pm ik_y$. The eigenenergies are

$$E_0(\mathbf{k}) = 0, \quad E_\pm(\mathbf{k}) = \frac{\epsilon_0}{2} \pm \sqrt{\frac{\epsilon_0^2}{4} + v_F^2 k^2}, \tag{5}$$

where $v_F = 3a\sqrt{t_1^2 + t_2^2}/2$. The resulting dispersion relation is plotted in Fig. 2.

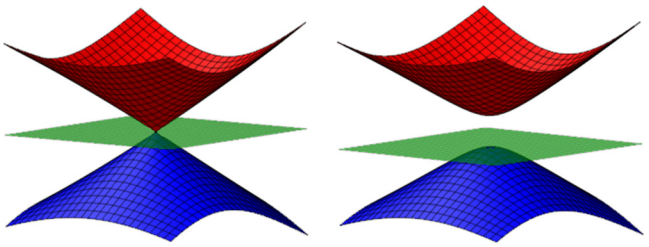

FIG. 2. The energy dispersion is sketched in the low-energy limit of the generalized α-T_3 model, Eq. (5) for $\epsilon_0 = 0$ (left) and $\epsilon_0 > 0$.

Similarly, around the $\mathbf{K}' = -\mathbf{K}$ point we have $f(\boldsymbol{K}'+\boldsymbol{k}) \approx -(3a/2)(k_x + ik_y)$ and thus, the Hamiltonian (3) for K' valley can be obtained by a unitary transformation with matrix U and a replacement of the parameters as

$$U = \begin{pmatrix} 0 & 0 & 1 \\ 0 & 1 & 0 \\ 1 & 0 & 0 \end{pmatrix} \quad \text{and} \quad (t_1, t_2) \to (-t_2, -t_1). \tag{6}$$

Note that in case of $t_1 = t_2$ and $\epsilon_0 = 0$ the contribution from the two valleys are identical, however, if either of these conditions are not met, this is not the case. Using the above U, one can easily calculate any operator or Green's function in valley K' from those in valley K, as we do so later on in Eq. (11).

When the on-site energy $\epsilon_0 = 0$ (Fig. 2), there are two special cases for this generalized model: (i) for $t_1 = t_2$, this equation reduces to the pseudospin-1 Dirac-Weyl model of Eq. (2) (see Refs. [12,15]) and (ii) for $t_2 = 0$ and $t_1 \neq 0$ (or the other way round) then it corresponds to the pseudospin-1/2 Dirac equation of Eq. (1) (i.e., the graphene) and contains a completely detached flat band.

For $\epsilon_0 \neq 0$, on the other hand, the model contains two parabolic bands, separated by a band gap of size $|\epsilon_0|$, and an additional flat band appear, touching the bottom or the top of one of the parabolic bands [14], depending on the sign of the local on-site energy term, as follows from Eq. (5) (see Fig. 2).

The pseudospin-1 Dirac-Weyl equation also describes the low-energy excitations in a Lieb lattice, and has been realized using photonic waveguides [16–18]. Recently, the DC Hall response and the optical conductivity without magnetic field of the α-T_3 lattice were studied in Ref. [15] without the local on-site energy term ϵ_0.

In this paper, we study the effect of quantizing magnetic field on Eq. (4). After determining the spectrum we present a novel method, which is based on the operator form of the Green's function of the system, which is independent from the chosen gauge or representation (i.e., position or momentum). To demonstrate the versatility of our method, we calculate the magneto-optical response of the generalized α-T_3 lattice, and reproduce known results along the way for graphene and the pseudospin-1 case with ease.

II. THE OPERATOR OF THE GREEN'S FUNCTION FOR THE GENERALIZED α-T_3 MODEL

To obtain the magneto-optical conductivity tensor $\boldsymbol{\sigma}(\omega)$ in magnetic field perpendicular to the plane of the dice lattice, one needs to calculate the Landau levels (LLs). As a standard procedure, replacing the canonical momentum by a gauge-invariant quantity $\hbar\mathbf{k} \to \boldsymbol{\Pi} = \hbar\mathbf{k} + |e|\mathbf{A}$ one finds the commutation relation $[\Pi_x, \Pi_y] = -i\hbar^2/l_B^2$, where $l_B = \sqrt{\frac{\hbar}{e|B|}}$ is the magnetic length scale, and $\mathbf{A}$ is the vector potential such that $\mathbf{B} = \boldsymbol{\nabla} \times \mathbf{A}$. By introducing the bosonic creation-annihilation operators $\hat{a} = \frac{l_B}{\hbar\sqrt{2}}(\Pi_x - i\Pi_y)$ and $\hat{a}^\dagger = \frac{l_B}{\hbar\sqrt{2}}(\Pi_x + i\Pi_y)$ we have $[a, a^\dagger] = 1$, and the Hamiltonian in

Eq. (4) becomes

$$H = \begin{pmatrix} 0 & \beta_1 \hat{a} & 0 \\ \beta_1 \hat{a}^\dagger & \epsilon_0 & \beta_2 \hat{a} \\ 0 & \beta_2 \hat{a}^\dagger & 0 \end{pmatrix}, \tag{7}$$

where $\beta_1 = (3c/\sqrt{2})\, t_1/l_B$ and $\beta_2 = (3c/\sqrt{2})\, t_2/l_B$ are the rescaled hopping elements t_1 and t_2, respectively.

Inspecting the Hamiltonian we assume that the eigenstate is of the form

$$|n,\zeta\rangle = (C_{\zeta,1}|n-1\rangle, C_{\zeta,2}|n\rangle, C_{\zeta,3}|n+1\rangle)^T, \tag{8}$$

where $|n\rangle$ is an eigenstate of the number operator $\hat{N} = \hat{a}^\dagger \hat{a}$ with $n = 0,1,2,\ldots$, while the band index is denoted by $\zeta = 0, \pm 1$, and $C_{\zeta,i}$ with $i = 1,2,3$ are coefficients to be determined from the eigenvalue problem of Hamiltonian (7). The Landau levels E_n^ζ and the corresponding states are given in Appendix A. The Landau levels are different at the K' valley but can be obtained from the above eigenvalues by the following replacement $(\beta_1, \beta_2) \to (-\beta_2, -\beta_1)$.

Now, we derive the Green's function defined by $G(z) = (z - H)^{-1}$. In contrast to the usual way where the Green's function is given in position representation, we give the operator form of the Green's function which is independent of any representation. We would like to emphasize that the operator form of the Green's function provides a great simplification in the calculation of different physical quantities involving the Green's function such as the magneto-optical conductivity. Usually, such quantities are expressed in terms of a trace of the product of the Green's function and other operators [in this work see Eq. (10b) as an example]. Now an accepted procedure is to use the position representation of the Green's function. However, this approach involves complicated analytical calculations. Indeed, for example Gusynin and Sharapov recently have used the position representation of the proper-time expression for the electron propagator for graphene [19,20] and bilayer graphene [21] in homogeneous magnetic field to calculate the magneto-optical conductivity. Using the Schwinger proper-time method [22] they derive the Fourier transform of the translation invariant part of the Green's function for single and bilayer graphene and presented a rather lengthy and complicated derivation to obtain the trace in the expression of the magneto-optical conductivity tensor. Finally, the evaluation of this trace including integrals of the generalized Laguerre polynomials requires further efforts to obtain analytical results. As we demonstrate below in contrast to this approach our results, namely the operator form of the Green's function gives an elegant way to calculate the trace using only the usual algebra of the creation and annihilation operators. We easily carried out the whole calculation for graphene using our method and found the same results presented in Refs. [19,20].

To show how effective our method is in this work, we calculate the magneto-optical conductivity tensor for the generalized α-T_3 model. To this end, we need the operator of the Green's function. After a lengthy but straightforward analytical calculation, we found for the K valley (for details see Appendix B):

$$G_K(z) = \begin{pmatrix} \frac{1}{z}\left[I + \beta_1^2 (\hat{N}+1) f_K(z,\hat{N}+1)\right] & \beta_1 \hat{a}\, f_K(z,\hat{N}) & \frac{\beta_1\beta_2}{z} \hat{a}^2 f_K(z,\hat{N}-1) \\ \beta_1 \hat{a}^\dagger f_K(z,\hat{N}+1) & z f_K(z,\hat{N}) & \beta_2 \hat{a}\, f_K(z,\hat{N}-1) \\ \frac{\beta_1\beta_2}{z} \hat{a}^{\dagger 2} f_K(z,\hat{N}+1) & \beta_2 \hat{a}^\dagger f_K(z,\hat{N}) & \frac{1}{z}\left[I + \beta_2^2 \hat{N} f_K(z,\hat{N}-1)\right] \end{pmatrix}, \tag{9a}$$

$$\text{where} \quad f_K(z,\hat{N}) = \left[z^2 - \epsilon_0 z - \beta_1^2 \hat{N} - \beta_2^2 (\hat{N}+1)\right]^{-1}, \tag{9b}$$

while $\hat{N} = \hat{a}^\dagger \hat{a}$ is the number operator, and I is the identity operator. The operator of the Green's function for the K' valley can be obtained by the transformation (6). We should emphasize that $f_K(z,\hat{N})$ is an operator but can easily be calculated in the Fock representation. Note that studying the poles of the Green's function we find the same Landau levels that are given in Appendix A.

III. MAGNETO-OPTICAL CONDUCTIVITY

Using the Kubo formula [23] the magneto-optical conductivity tensor in the bubble approximation can be obtained from the operator of the Green's function given by Eq. (9) in the following way:

$$\sigma_{\alpha\beta}(\xi) = \frac{\Pi_{\alpha\beta}(\xi) - \Pi_{\alpha\beta}(0)}{\xi}, \tag{10a}$$

$$\text{where} \quad \Pi_{\alpha\beta}(i\nu_m) = \frac{i k_B T}{2\pi l_B^2} \sum_{k=-\infty}^{\infty} \mathrm{Tr}(j_\alpha G(i\omega_k + i\nu_m) \times j_\beta G(i\omega_k)). \tag{10b}$$

Here, $\Pi_{\alpha\beta}$ is the current-current correlation function ($\alpha,\beta = x,y$), $\omega_k = (2k+1)\pi k_B T$ are the fermionic Matsubara frequencies (here k_B is the Boltzmann constant, T is the temperature and k is an integer) and $\nu_m = 2m\pi k_B T$ are bosonic Matsubara frequencies (m is an integer). The trace can be obtained using the eigenstates of the Landau levels given in Appendix A. The sum over the fermionic Matsubara frequencies ω_k in (10b) can be performed by the usual summation method [23]. Finally, the current density operator $\mathbf{j} = \frac{e}{\hbar} \frac{\partial H_K}{\partial \mathbf{k}}$ with Hamiltonian (4) at the K valley is given by

$$j_x = \frac{e l_B}{\sqrt{2}\hbar} \begin{pmatrix} 0 & \beta_1 & 0 \\ \beta_1 & 0 & \beta_2 \\ 0 & \beta_2 & 0 \end{pmatrix}, \quad j_y = \frac{i e l_B}{\sqrt{2}\hbar} \begin{pmatrix} 0 & -\beta_1 & 0 \\ \beta_1 & 0 & -\beta_2 \\ 0 & \beta_2 & 0 \end{pmatrix}, \tag{11}$$

while at the K' valley it is given by the transformation (6).

Then, the frequency-dependent magneto-optical conductivity tensor $\boldsymbol{\sigma}(\omega)$ can be calculated from Eq. (10a) using the usual analytic continuation [23] $i\nu_m \to \omega + i\eta$ in the current-current correlation function $\Pi_{\alpha\beta}(i\nu)$ given by Eq. (10b), where η is the inverse life time of the particle.

IV. RESULTS: THE MAGNETO-OPTICAL CONDUCTIVITY

In this section, we present our results for the magneto-optical conductivity. The analytical calculation can be carried out in a straightforward way using the algebra of the creation and annihilation operators. Our results show explicitly the different contributions to the conductivity corresponding to the interband and intraband transitions between the flat band and a cone, and between cones in each valley. Below the dependence of the conductivity on the frequency, the temperature, the magnetic field and the Fermi energy will be discussed. Moreover, from these results we shall establish the selection rules for the possible optical excitations between Landau levels. In addition, once the Green's functions are calculated within our formalism, any response function follows straightforwardly, not just the conductivities. First, we consider the longitudinal conductivity.

A. The longitudinal conductivity

The total longitudinal conductivity can be written as the sum of terms corresponding to intraband and interband transitions. After a lengthy but straightforward analytical calculation, we find

$$\sigma_{xx}(\omega) = \sum_{\zeta=\pm} \left(\sigma^{K,\zeta}_{xx,f-c} + \sigma^{K,\zeta}_{xx,c-c,\text{inter}} + \sigma^{K,\zeta}_{xx,c-c,\text{intra}}\right) + \left(\beta_1^2 \leftrightarrow \beta_2^2\right), \tag{12}$$

where $\sigma^{K,\zeta}_{xx,f-c}$, $\sigma^{K,\zeta}_{xx,c-c,\text{inter}}$, and $\sigma^{K,\zeta}_{xx,c-c,\text{intra}}$ are the contributions to the total longitudinal conductivity from the interband transitions between the flat band and a cone, the interband transitions between cones, and the intraband transitions (within the cones) in the K valley, respectively and are given in Appendix C. The contribution to the conductivity from the K' valley is given by the second term in (12) indicated by the replacement $\beta_1^2 \leftrightarrow \beta_2^2$.

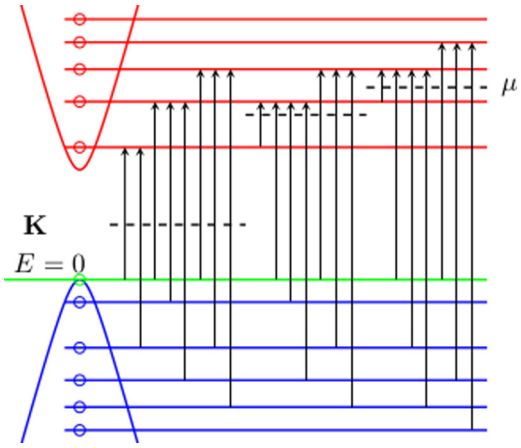

FIG. 3. Allowed transitions for different values of the Fermi energy.

To see the allowed transitions between different Landau levels we consider the three contributions to the conductivity given by Eq. (12). The first term corresponds to the transition from flat band ($\zeta = 0$) to cone ($\zeta = 1$) and at zero temperature the difference of the two Fermi functions becomes nonzero if the Landau level indices n of the two energy levels differ exactly by one. For finite temperature in principle other types of transitions are also allowed but much smaller than the ones mentioned above. The other selection rules can be obtained from the second and third terms in the expression of the conductivity.

The magnitude of the contribution corresponding to a transition with energy $E \approx \hbar\omega$ at frequency ω is approximately the prefactor of the term $\frac{1}{(\hbar\omega - E)^2 + \eta^2}$ (for not too small values of the magnetic field and for $\mu, \omega > 0$). In particular, for the transitions from the flat band to the cone band this is

$$\text{Re}\sigma_{xx}(\omega = E_m^+/\hbar) \approx \frac{e^2}{\eta h}\left(\frac{\beta_1^2 + \beta_2^2 + \frac{(m+1)\beta_1^4}{E^+_{m+1}E^-_{m+1}} + \frac{m\beta_2^4}{E^+_{m-1}E^-_{m-1}}}{E_m^+ - E_m^-} + \left(\beta_1^2 \leftrightarrow \beta_2^2\right)\right), \tag{13a}$$

which in case of $\beta_1 = \beta_2$ reads as

$$\text{Re}\sigma_{xx}(\omega = E_m^+/\hbar) \approx \frac{e^2\beta_1^2}{\eta h E_m^+}\frac{4m^2 + 4m - 5}{4m^2 + 4m - 3}. \tag{13b}$$

For the amplitudes of transitions between the cone bands $\zeta = -1$ and $\zeta = +1$, one finds

$$\text{Re}\sigma_{xx}(\omega = (E^+_{m+1} - E^-_m)/\hbar) \approx \frac{e^2}{\eta h}\sum_{\zeta=\pm}\frac{\zeta(m+1)\left(\beta_1^2 E_m^\zeta + \beta_2^2 E_{m+1}^{-\zeta}\right)^2}{\left(E_m^\zeta - E_m^{-\zeta}\right)\left(E_{m+1}^\zeta - E_{m+1}^{-\zeta}\right)\left(-E_m^\zeta E_{m+1}^{-\zeta}\right)\left(E_m^\zeta - E_{m+1}^{-\zeta}\right)} + \left(\beta_1^2 \leftrightarrow \beta_2^2\right), \tag{14a}$$

which in case of $\beta_1 = \beta_2$ takes the form

$$\text{Re}\sigma_{xx}(\omega = (E^+_{m+1} - E^-_m)/\hbar) \approx \frac{e^2\beta_1^2}{\eta h}\frac{1}{E_m^+ - E^-_{m+1}}\frac{(m+1)(2(m+1) - \sqrt{(2m+1)(2m+3)})}{(2m+1)(2m+3)}. \tag{14b}$$

It is easy to check that the contributions of the transitions from flat to cone bands are significantly larger than the ones corresponding to cone to cone interband transitions when $t_1 = t_2$ (or more generally, when the two hoppings are sufficiently close to each other which is the case in Fig. 4). However, as soon as, e.g., $t_2 = 0$, the conventional graphene case is recovered without any flat band, and only cone to cone transitions remain present. In summary, in Figs. 3 and 4, we illustrate the allowed transitions

for different Fermi energies. Figure 4 shows the conductivities as a function of the frequency $\Omega = \hbar\omega$ for three different chemical potential μ.

For $\mu = 50$ K, the transition $|n = 1,\zeta = 0\rangle \to |n = 0,\zeta = 1\rangle$ gives the two largest peaks in the conductivity corresponding to the two valleys. While in case of $\mu = 500$ K the transition $|n = 0,\zeta = 1\rangle \to |n = 1,\zeta = 1\rangle$ provides the largest peaks in the conductivity. Finally, for $\mu = 700$ K, the Landau level indices change as $n = 1 \to n = 2$ for K valley and $n = 0 \to n = 1$ for K' valley but the quantum number $\zeta = 1$ does not change.

Finally, we discuss the dependence of magneto-optical conductivity on external field. It is clear that for $B \to \infty$ the conductivity should vanish since the distance between the Landau levels tend to infinity. The formula for the low-field limit is obtained by introducing the variable $\Omega = E_n^+ - \epsilon_0/2$ and replacing the summation over n into a integral as follows:

$$\sigma_{xx} = \frac{2ie^2\xi}{h}\int_{\epsilon_0/2}^{\infty} d\Omega\left\{\frac{\left(\frac{\epsilon_0}{2}\right)^2 + \Omega^2\cos^2(2\phi)}{\Omega^2}\frac{n_F\left(\frac{\epsilon_0}{2}-\Omega\right) - n_F\left(\frac{\epsilon_0}{2}+\Omega\right)}{\xi^2 - 4\Omega^2} + \sin^2(2\phi)\left[\frac{n_F(0) - n_F\left(\frac{\epsilon_0}{2}+\Omega\right)}{\xi^2 - \left(\frac{\epsilon_0}{2}+\Omega\right)^2}\right.\right.$$
$$\left.\left. - \frac{n_F(0) - n_F\left(\frac{\epsilon_0}{2}-\Omega\right)}{\xi^2 - \left(\frac{\epsilon_0}{2}-\Omega\right)^2}\right] + \frac{\Omega^2 - \left(\frac{\epsilon_0}{2}\right)^2}{\Omega\xi^2}\left[\frac{\partial n_F\left(\frac{\epsilon_0}{2}-\Omega\right)}{\partial\Omega} - \frac{\partial n_F\left(\frac{\epsilon_0}{2}+\Omega\right)}{\partial\Omega}\right]\right\}, \tag{15}$$

where $\tan\phi = t_2/t_1$. In case of $\phi = \pi/4$ (i.e., when $t_1 = t_2$) and $\epsilon_0 = 0$, Eq. (15) transforms into Eq. (21) of Ref. [10] and in case of $\phi = \pi/2$ (graphene) and $\epsilon_0 = 0$ into Eq. (13) of Ref. [20].

As far as intermediate magnetic fields are concerned, the height of the peaks and their positions can be determined from the results given by Eqs. (C1). For simplicity, here we only consider the case $\beta_1 = \beta_2$. In fact, the pattern for general hopping amplitudes is rather cumbersome as peak energies corresponding to different transitions might coincide (approximately) and producing a higher peak together (see Fig. 5), even for very small values of the scattering rate. Let us consider the case when $0 < \mu < E_0^+$ so that we do not have to deal with the single intraband transition. It is also allowed to neglect cone-to-cone interband peaks according to the arguments above. However, we should be careful when we consider the low-field limits since in this case the main contribution to the peaks in the conductivity results from more than one transitions between the LLs. The value of the real part of the longitudinal conductivity tends to the low magnetic field limit that can be determined from the integral in Eq. (15).

Therefore main characteristics of the oscillation of the longitudinal conductivity as a function of the magnetic field is mainly governed by the transitions between the flat band to cone levels. For a fixed value of frequency ω, the mth peak (starting from the left-hand side in Fig. 5) occurs at $B_m^{-1/2} = \frac{\gamma}{\omega}\sqrt{2m+1}$, where $\gamma = \beta_1/\sqrt{B}$ independent of the magnetic field. So the distance between peaks decreases as the difference of the square root of two neighboring odd numbers. The amplitude of the oscillations is given by Eqs. (13a) and (13b), which implies that for large enough magnetic field the peaks in the longitudinal conductivity tends to

$$\mathrm{Re}\sigma_{xx}(\omega = E_m^+/\hbar) \approx \frac{e^2}{\eta h}\frac{\gamma^2 B_m}{\omega}, \tag{16}$$

which is proportional to the position of the peaks B_m.

B. The transversal conductivity

Similarly to the case of longitudinal conductivity the transversal conductivity (off-diagonal component of the conductivity tensor $\boldsymbol{\sigma}$) can also be written as the sum of terms corresponding to intraband and interband transitions. After a lengthy but straightforward analytical calculation, we find

$$\sigma_{xy}(\omega) = \sum_{\zeta=\pm}\left(\sigma_{xy,f-c}^{K,\zeta} + \sigma_{xy,c-c,\mathrm{inter}}^{K,\zeta} + \sigma_{xy,c-c,\mathrm{intra}}^{K,\zeta}\right) + \left(\beta_1^2 \leftrightarrow \beta_2^2\right), \tag{17}$$

where $\sigma_{xy,f-c}^{K,\zeta}$, $\sigma_{xy,c-c,\mathrm{inter}}^{K,\zeta}$, and $\sigma_{xy,c-c,\mathrm{intra}}^{K,\zeta}$ are the contributions to the total transversal conductivity from the interband transitions between the flat band and a cone, the interband transitions between cones, and the intraband transitions (within the cones) in the K valley, respectively and are given in Appendix C. The contribution to conductivity from the K' valley is given by the second term in (17) indicated by the replacement $\beta_1^2 \leftrightarrow \beta_2^2$.

Figure 6 shows the Hall conductivity (the imaginary part of the off-diagonal component of the conductivity tensor) as a function the frequency for different chemical potential (in panel a) and for different hopping amplitudes (in panel b). When $0 < \mu < E_0^+$ in a valley (blue solid line) then there is no intraband transition so peaks in the conductivity result only from flat band to cone and cone to cone transitions. In this case, there is a negative peak (around $\Omega \approx 400$ K in the figure) corresponding to the transition $|n = 1,\zeta = 0\rangle \to |n = 0,\zeta = 1\rangle$. All the other peaks corresponding to other flat band to cone transitions are positive. Small negative peaks (around $\Omega \approx 300$ K in the figure) due to interband cone to cone transitions are also present. However, if $E_0^+ < \mu < E_1^+$ (red dashed line), then the aforementioned negative peak from flat band to cone transition disappears, while another negative peak appears due to an intraband transition.

The height of a peak at frequency ω corresponding to a transition with energy $E \approx \hbar\omega$ is approximately the weight factor of the term $\frac{1}{(\hbar\omega - E)^2 + \eta^2}$ (again, for not too small values of the magnetic field and for $\mu, \omega > 0$). The heights of positive peaks (flat band to cone transitions) fall rapidly in both cases

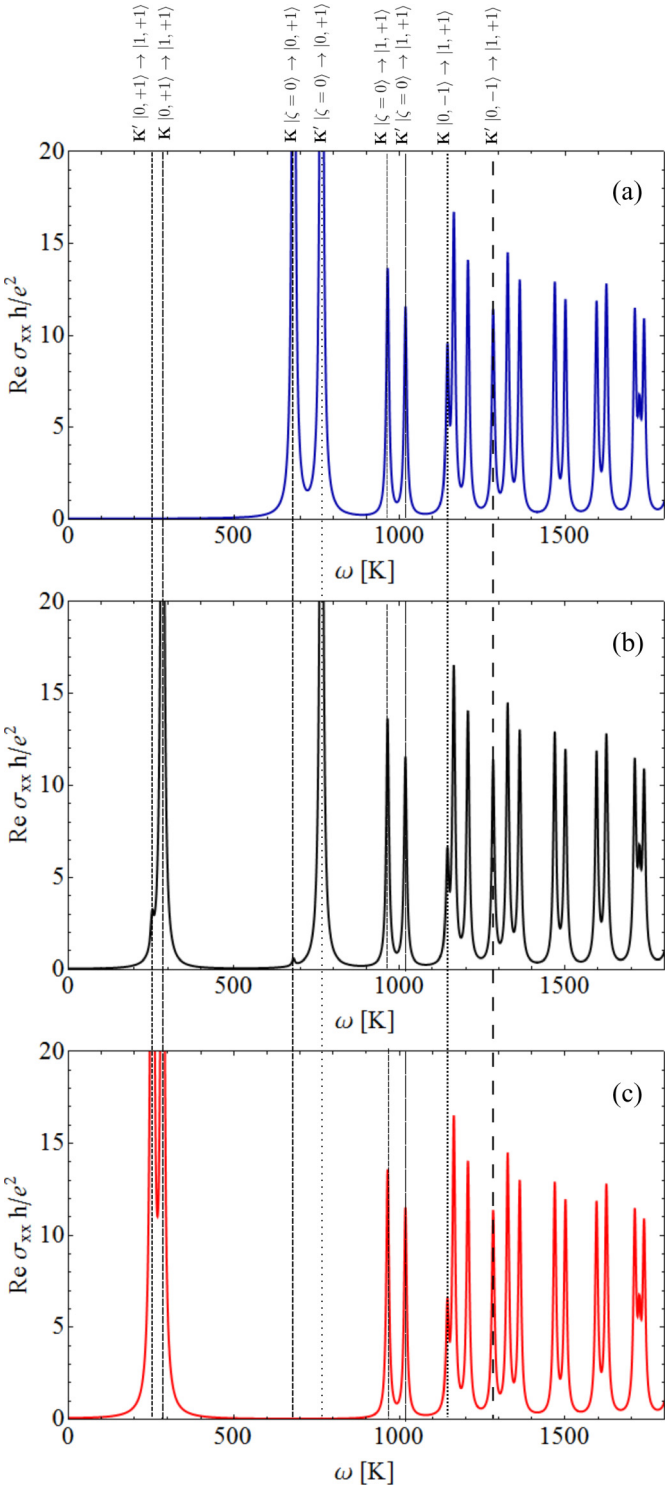

FIG. 4. The real part of the longitudinal conductivity (in units of e^2/h) as a function of the frequency ω (in units of K) for Fermi energy $\mu = 500$ K [blue line, (a)] which is in the gap, $\mu = 730$ K [black line, (b)] which lies between the Landau levels $n = 0$ and $n = 1$ in the K valley and in the gap in the K' valley, and $\mu = 850$ K [red line, (c)], which is between the Landau levels $n = 0$ and $n = 1$ for both valleys. The parameters are $T = 10$ K, $\epsilon_0 = 500$, $\beta_1 = 350$ K, $\beta_2 = 450$ K, and $\eta = 5$ K. For the first few peaks, the corresponding transitions are assigned in the form of $|n,\zeta\rangle \to |n',\zeta'\rangle$.

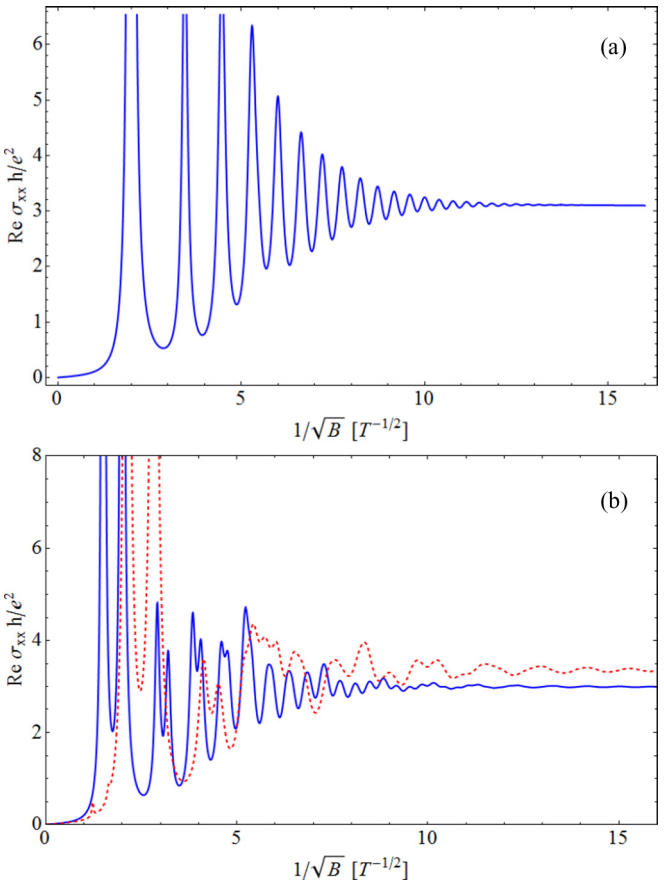

FIG. 5. The real part of the longitudinal conductivity (in units of e^2/h) as a function of the inverse square root of magnetic field B (here B is in units of T) for (a) $\beta_1 = \beta_2 = 400$ K $\sqrt{B}$, (b) $\beta_1 = 300$ K $\sqrt{B}$ and $\beta_2 = 400$ K $\sqrt{B}$ for the blue solid line, $\epsilon_0 = 100$ K for the red dotted line. The parameters are $T = 10$ K, $\mu = 50$ K, $\omega = 200$ K, $\eta = 5$ K, and $\epsilon_0 = 0$ in both cases.

in terms of the frequency according to

$$\mathrm{Im}\sigma_{xy}(\omega = E_m^+/\hbar) \approx \frac{e^2}{\eta h}\left(\frac{\beta_2^2 - \beta_1^2 + \frac{m\beta_2^4}{E_{m-1}^+ E_{m-1}^-} - \frac{(m+1)\beta_1^4}{E_{m+1}^+ E_{m+1}^-}}{E_m^+ - E_m^-} + \left(\beta_1^2 \leftrightarrow \beta_2^2\right)\right), \tag{18a}$$

which in case of $\beta_1 = \beta_2$ reads as

$$\mathrm{Im}\sigma_{xy}(\omega = E_m^+/\hbar) \approx \frac{e^2\beta_1^2}{\eta h E_m^+}\frac{2m+1}{4m^2+4m-3}. \tag{18b}$$

It is also worth noting that when $\beta_1 \neq \beta_2$ then the first negative flat band to cone peak splits into two peaks (corresponding to K and K' valleys, respectively) as shown in Fig. 6(a) around $\Omega \approx 250$ K. If the difference between the two hopping amplitudes are large enough then it might occur that one of these two peaks becomes positive as can be seen in Fig. 7 exactly at $\Omega = 300$ K.

Similarly, it is easy to check that the peaks corresponding to cone-to-cone interband and intraband transitions are always negative. The heights of peaks for interband cone-to-cone transitions ($\hbar\omega = E^+_{m+1} - E^-_m = E^+_m - E^-_{m+1}$) are

$$\mathrm{Im}\sigma_{xy}(\omega = (E^+_{m+1} - E^-_m)/\hbar) \approx -\frac{e^2}{\eta h}\sum_{\zeta=\pm}\frac{\zeta(m+1)\left(\beta_1^2 E_m^{\zeta} + \beta_2^2 E_{m+1}^{-\zeta}\right)^2}{\left(E_m^{\zeta} - E_m^{-\zeta}\right)\left(E_{m+1}^{\zeta} - E_{m+1}^{-\zeta}\right)\left(-E_m^{\zeta}E_{m+1}^{-\zeta}\right)\left(E_m^{\zeta} - E_{m+1}^{-\zeta}\right)} + \left(\beta_1^2 \leftrightarrow \beta_2^2\right) \tag{19}$$

and for intraband transitions

$$\mathrm{Im}\sigma_{xy}(\omega = (E^+_{m+1} - E^-_m)/\hbar) \approx -\frac{e^2}{\eta h}\frac{(m+1)\left(\beta_1^2 E_m^{+} + \beta_2^2 E_{m+1}^{+}\right)^2}{(E_m^{+} - E_m^{-})(E_{m+1}^{+} - E_{m+1}^{-})(E_m^{+}E_{m+1}^{+})(E_{m+1}^{+} - E_m^{+})} + \left(\beta_1^2 \leftrightarrow \beta_2^2\right). \tag{20}$$

Finally, we consider the transversal conductivity in the dc limit ($\omega = 0$) and at zero temperature. In this case we obtain the usual Hall conductivity. From Eq. (C2), we can find the contribution from the K and K' valleys as

$$\sigma_{xy}^{K} = \frac{e^2}{h}\left(\frac{\beta_1^2 - \beta_2^2}{\beta_1^2 + \beta_2^2}F(0) - 2\sum_{n=0}^{\infty}F_n^K\right), \tag{21a}$$

$$\sigma_{xy}^{K'} = \frac{e^2}{h}\left(\frac{\beta_2^2 - \beta_1^2}{\beta_1^2 + \beta_2^2}F(0) - 2\sum_{n=0}^{\infty}F_n^{K'}\right), \tag{21b}$$

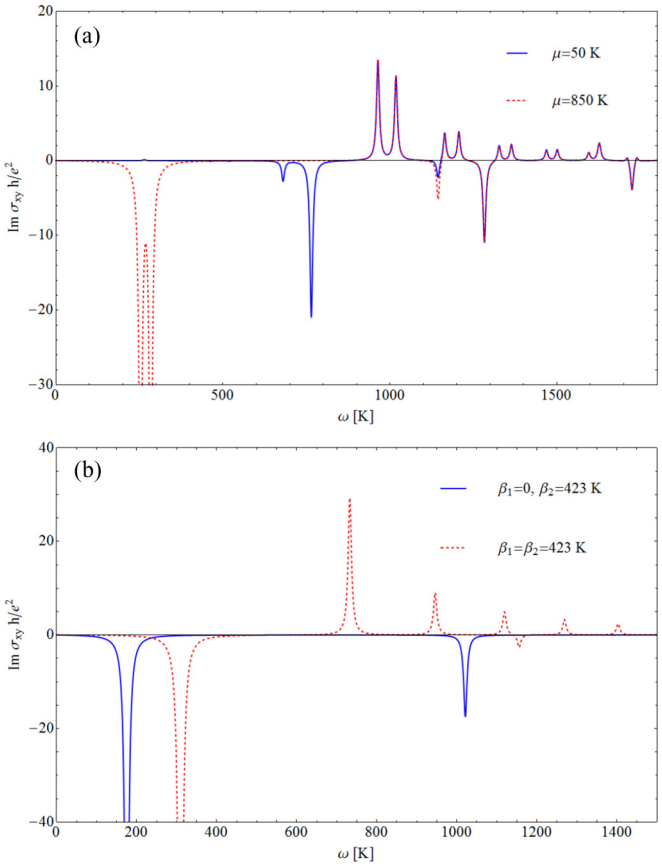

FIG. 6. The imaginary part of the transversal conductivity (in units of e^2/h) as a function of the frequency $\Omega = \hbar\omega/k_B$ (in units of K) (a) for Fermi energy $\mu = 50$ K lying between the flat band and the first LL (blue solid line) and $\mu = 500$ K which is between the first and second LL (red dashed line), (b) for $\mu = 50$ K and for two sets of hopping parameters: $\epsilon_0 = \beta_1 = 0$, $\beta_2 = 423$ K corresponding to graphene with $B = 1$ T magnetic field (blue solid line), and $\epsilon_0 = 0$, $\beta_1 = \beta_2 = 423$ K related to the Dirac-Weyl model for s=1 (red dashed line). The parameters are T=10 K and η=5 K in both cases.

where $F_n^K = n_F(E_n^+) + n_F(E_n^-)$ and $E_n^{\pm}$ are the energy levels for the K valley, and $F_n^{K'}$ is the same as F_n^K with energy levels for the K' valley. Our valley resolved results for $\epsilon_0 = 0$ differ from those in Ref. [15], obtained using the Streda formula. although the total, $K + K'$ contributions do agree. Note that the Streda formula calculation also fails to reproduce the half-integer quantized Hall response of graphene though. Here the spin degeneracy is taken into account. Thus the total contributions from K and K' valleys can be rewritten as

$$\sigma_{xy}(\mu, B, T) = \sigma_{xy}^{K} + \sigma_{xy}^{K'} = -\frac{2e^2}{h}\sum_{n=0}^{\infty}\left(F_n^K + F_n^{K'}\right). \tag{22}$$

The Hall conductivity as a function of the Fermi energy at zero temperature and in DC limit is plotted in Figs. 8 and 9. The insets in this figure show the individual contributions from the two valleys to the conductivity. It can be shown that the conductivity is zero when μ is in the narrower energy interval $\{E_0^-, E_0^+\}$ corresponding to the K and K' valleys. For parameters used in the figure this is $|\mu| < \beta_1$. Moreover, the conductivity has a change $2e^2/h$ at all the other Landau levels. For $\epsilon_0 \neq 0$, the Hall conductivity looses its symmetry with respect to $\mu = 0$. Our results for $\epsilon_0 = 0$ agree with those on Ref. [24].

We now show that this Hall conductivity can be related to the Berry phase. Indeed, when the temperature is zero and the Fermi energy lies between the flat band and first LL then the sums in Eq. (21) becomes zero and $F(0) = 2$. Then the

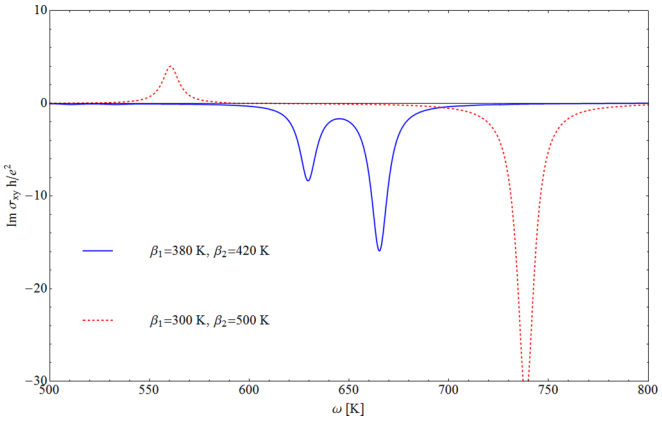

FIG. 7. The imaginary part of the transversal conductivity (in units of e^2/h) as a function of the frequency $\Omega = \hbar\omega/k_B$ (in units of K), for hopping amplitudes $\epsilon_0 = 0$, $\beta_1 = 380$ K, $\beta_2 = 420$ K (blue solid line), and for $\epsilon_0 = 0$, $\beta_1 = 300$ K, $\beta_2 = 500$ K (red dashed line). The parameters are $T = 10$ K and $\eta = 5$ K.

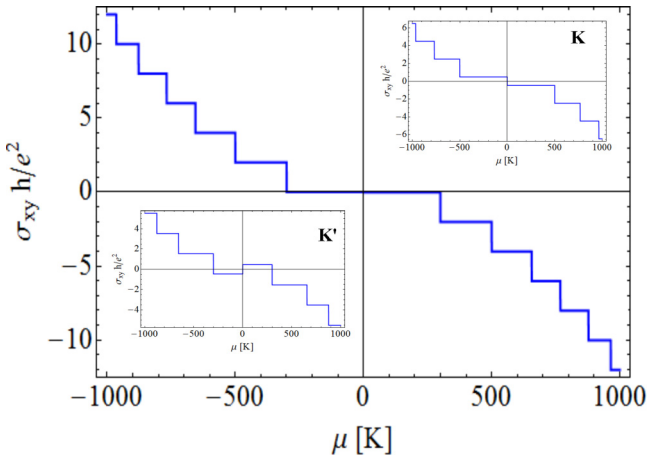

FIG. 8. The transversal conductivity (in units of e^2/h) in dc limit ($\omega = 0$) as a function of the Fermi energy. Insets (upper right and lower left) show the contributions from the K and K' valleys, respectively. The parameters are $T = 0.01$ K, $\eta = 5$ K, $\epsilon_0 = 0$, $\beta_1 = 300$ K, and $\beta_2 = 500$ K.

conductivity becomes

$$\sigma_{xy}^{K,K'} = \pm 2\,\frac{e^2}{h}\,\frac{\beta_1^2 - \beta_2^2}{\beta_1^2 + \beta_2^2} = \pm 2\,\frac{e^2}{h}\cos(2\phi), \qquad (23)$$

where ϕ is given by $\tan\phi = t_2/t_1$ and the spin degeneracy is included. This results is in agreement with the Berry phases obtained in Refs. [12,15]. It is interesting to note that the valley resolved Hall response is not only *fractional* but can also be rational without any electron-electron interactions, albeit the sum of the two valleys, the total Hall response is always integer quantized.

V. CONCLUSIONS

In this work, the magneto-optical conductivity in the generalized α-T_3 model is calculated. In this generalized form we assumed that the on-site energy ϵ_0 of the sixfold connected site can be nonzero. Using the Kubo formula expressed with Green's function, the magneto-optical conductivity tensor is calculated as functions of frequency, external field, temperature and Fermi energy. To this end, we introduce a new analytical procedure to determine the Green's function in an operator form independent of any representation. When the Green's function is given in position representation the evaluation of the trace in the Kubo formula is a quite cumbersome analytical calculation. The advantage of our approach is that the Kubo formula can be calculated in simple way using only the algebra of the creation and annihilation operators. To demonstrate the theoretical method mentioned above, the calculations are also carried out for graphene and it is shown that the results obtained from our method are in agreement with those known in the literature.

From our general result for the transversal conductivity we derived an analytic expression for the Hall-conductivity in dc limit. We show that the Hall conductivity at zero temperature agrees with that obtained from the Berry phase calculated in earlier works. Moreover, the Hall conductivity is integer quantized and the steps of quanta depend continuously on the hopping parameters between adjacent layers.

We believe that our predictions for the magneto-optical conductivity can be tested experimentally with cold atoms in an optical lattice. Furthermore, our algorithm is an efficient and universal approach and thus easily applicable to other systems.

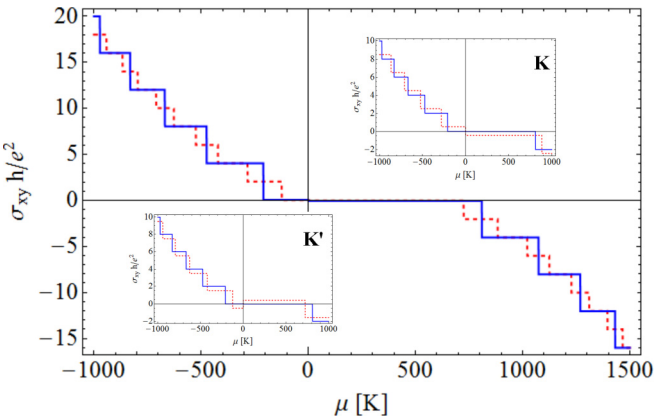

FIG. 9. The transversal conductivity (in units of e^2/h) in dc limit ($\omega = 0$) as a function of the Fermi energy (spin degeneracy factor included!). Insets (upper right and lower left) show the contributions from the K and K' valleys, respectively. The parameters are $T = 0.01$ K, $\eta = 5$ K, $\epsilon_0 = 600$ K, $\beta_1 = 300$ K, $\beta_2 = 500$ K for the red dotted line and $\epsilon_0 = 600$ K, $\beta_1 = \beta_2 = 412$ K for the blue solid line, so that $\beta_1^2 + \beta_2^2$ has the same value for the two cases.

ACKNOWLEDGMENTS

We would like to thank A. Pályi for helpful discussions. This work is supported by The National Research, Development and Innovation Office under Contracts No. 119442, No. 105149 and No. 108676.

APPENDIX A: EIGENVALUES AND EIGENSTATES OF THE SYSTEMS

In this section, we present the eigenvalues and the eigenstates of the Hamiltonian (7) (around the K valley). The Schrödinger equation reads as

$$H|n,\zeta\rangle = E_n^\zeta |n,\zeta\rangle, \qquad (A1)$$

where E_n^ζ and $|n,\zeta\rangle$ is the energy eigenvalue and the corresponding eigenstate, respectively, and $n = 0,1,2,\ldots$ and $\zeta = -1,0,+1$ denote the Fock number and the band index, respectively. To solve this equation, we look for a solution of the form given by Eq. (8). The results are summarized in Table I.

APPENDIX B: CALCULATION OF THE GREEN'S FUNCTION

To obtain the operator of the Green's function for the Hamiltonian H given by Eq. (7), we partitioned the operator $z - H$ as

$$z - H = \left(\begin{array}{cc|c} z & -\beta_1\,\hat{a} & 0 \\ -\beta_1\,\hat{a}^\dagger & z-\epsilon_0 & -\beta_2\,\hat{a} \\ \hline 0 & -\beta_2\,\hat{a}^\dagger & z \end{array}\right) \equiv \begin{pmatrix} A & B \\ C & D \end{pmatrix}. \qquad (B1)$$

TABLE I. Landau levels and eigenstates for valley K. Each levels are labeled by the Fock number n and a band index ζ. The normalization factors are $\gamma_n^\zeta = (\beta_1^2 n + \beta_2^2(n+1) + (E_n^\zeta)^2)^{-\frac{1}{2}}$ for $\zeta = \pm$ and $\gamma_n^0 = (\beta_1^2 n + \beta_2^2(n+1))^{-\frac{1}{2}}$ for $\zeta = 0$.

n,ζ	E_n^ζ	$\lvert n,\zeta\rangle$
$n>0,\zeta=\pm1$	$E_n^{\pm1} = \frac{\epsilon_0}{2} + \zeta\sqrt{\left(\frac{\epsilon_0}{2}\right)^2 + \beta_1^2 n + \beta_2^2(n+1)}$	$\gamma_n^{\pm1}(\beta_1\sqrt{n}\lvert n-1\rangle, E_n^{\pm1}\lvert n\rangle, \beta_2\sqrt{n+1}\lvert n+1\rangle)^T$
$n>0,\zeta=0$	$E_n^0 = 0$	$\gamma_n^0(-\beta_2\sqrt{n+1}\lvert n-1\rangle, 0, \beta_1\sqrt{n}\lvert n+1\rangle)^T$
$n=0,\zeta=\pm1$	$E_0^{\pm1} = \frac{\epsilon_0}{2} + \zeta\sqrt{\left(\frac{\epsilon_0}{2}\right)^2 + \beta_2^2}$	$\gamma_0^{\pm1}(0, E_0^{\pm1}\lvert 0\rangle, \beta_2\lvert 1\rangle)^T$
$n=0,\zeta=0$	$E_0^0 = 0$	$(0,0,\lvert 0\rangle)^T$

Then we apply the general formula for the inverse of a 2×2 partitioned matrix

$$\begin{pmatrix} A & B \\ C & D \end{pmatrix}^{-1} = \begin{pmatrix} A^{-1} + A^{-1}BS^{-1}CA^{-1} & -A^{-1}BS^{-1} \\ -S^{-1}CA^{-1} & S^{-1} \end{pmatrix}, \tag{B2}$$

where $S = D - CA^{-1}B$ and the operators A and S can be inverted. This is often called in the literature the Banachiewicz inversion formula [25,26].

The inverse of operator A defined in (B1) can also be calculated from formula (B2) and after a simple algebra we find

$$A^{-1} = \begin{pmatrix} (z-\epsilon_0)\,p(z,\hat{N}+1) & \beta_1\,\hat{a}\,p(z,\hat{N}) \\ \beta_1\,\hat{a}^\dagger\,p(z,\hat{N}+1) & z\,p(z,\hat{N}) \end{pmatrix}, \tag{B3}$$

where $p(z,\hat{N}) = (z^2 - \epsilon_0 z - \beta_1^2\hat{N})^{-1}$ and $\hat{N} = \hat{a}^\dagger\hat{a}$ is the number operator. Now using (B3) and the general formula (B2) the matrix elements of the inverse of matrix in (B1) can be calculated analytically, and we find

$$S^{-1} = \frac{1}{z}\big(I + \beta_2^2 N f(z,\hat{N}-1)\big), \tag{B4a}$$

$$-A^{-1}BS^{-1} = \begin{pmatrix} \frac{\beta_1\beta_2}{z}\,\hat{a}^2 f(z,\hat{N}-1) \\ \beta_2\,\hat{a}\,f(z,\hat{N}-1) \end{pmatrix}, \tag{B4b}$$

$$-S^{-1}CA^{-1} = \left(\frac{\beta_1\beta_2}{z}\,\hat{a}^{\dagger2} f(z,\hat{N}+1),\, \beta_2\,\hat{a}^\dagger f(z,\hat{N})\right), \tag{B4c}$$

$$A^{-1} + A^{-1}BS^{-1}CA^{-1} = \begin{pmatrix} \frac{1}{z}\big[I + \beta_1^2(\hat{N}+1)f(z,\hat{N}+1)\big] & \beta_1\,\hat{a}\,f(z,\hat{N}) \\ \beta_1\,\hat{a}^\dagger f(z,\hat{N}+1) & z f(z,\hat{N}) \end{pmatrix}, \tag{B4d}$$

where $f(z,\hat{N}) = [z^2 - \epsilon_0 z - \beta_1^2\,\hat{N} - \beta_2^2(\hat{N}+1)]^{-1}$.

Here we have made use of the following identities:

$$\hat{a}\,f(z,\hat{N}) = f(z,\hat{N}+1)\,\hat{a}^\dagger, \tag{B5}$$

$$\hat{a}^\dagger\,f(z,\hat{N}) = f(z,\hat{N}-1)\,\hat{a}. \tag{B6}$$

Finally, substituting the terms given by Eqs. (B4) into Eq. (B2), we obtain the operator of the Green's function $G(z) = (z-H)^{-1}$ as given by Eq. (9). For the case of K' valley, the Green's function can be obtained by the transformation (6).

APPENDIX C: EXPRESSIONS FOR THE LONGITUDINAL AND TRANSVERSAL CONDUCTIVITIES

Using the operator form of the Green's function given by Eq. (9) and the current operators (11), and performing the Matsubara summation in (10b) the magneto-optical conductivity can be calculated analytically. Then the longitudinal conductivity is given by Eq. (12) in which the different terms reads

$$\sigma_{xx,f-c}^{K,\zeta}(\omega) = \frac{ie^2}{h}\sum_{n=0}^{\infty}\frac{\beta_1^2+\beta_2^2+\frac{(n+1)\beta_1^4}{E_{n+1}^+E_{n+1}^-}+\frac{n\beta_2^4}{E_{n-1}^+E_{n-1}^-}}{E_n^\zeta - E_n^{-\zeta}}\left(\frac{1}{\xi - E_n^\zeta}+\frac{1}{\xi+E_n^\zeta}\right)\big[n_{\rm F}(0) - n_{\rm F}(E_n^\zeta)\big], \tag{C1a}$$

$$\sigma_{xx,c-c,\rm inter}^{K,\zeta}(\omega) = \frac{ie^2}{h}\sum_{n=0}^{\infty}\frac{(n+1)\big(\beta_1^2E_n^\zeta + \beta_2^2E_{n+1}^{-\zeta}\big)^2}{\big(E_n^\zeta - E_n^{-\zeta}\big)\big(E_{n+1}^\zeta - E_{n+1}^{-\zeta}\big)\big(-E_n^\zeta E_{n+1}^{-\zeta}\big)\big(E_n^\zeta - E_{n+1}^{-\zeta}\big)} \times\left(\frac{1}{\xi+E_n^\zeta - E_{n+1}^{-\zeta}}+\frac{1}{\xi - E_n^\zeta + E_{n+1}^{-\zeta}}\right)\big[n_{\rm F}(E_{n+1}^{-\zeta}) - n_{\rm F}(E_n^\zeta)\big], \tag{C1b}$$

$$\sigma_{xx,c-c,\rm intra}^{K,\zeta}(\omega) = \frac{ie^2}{h}\sum_{n=0}^{\infty}\frac{(n+1)\big(\beta_1^2E_n^\zeta + \beta_2^2E_{n+1}^{\zeta}\big)^2}{\big(E_n^\zeta - E_n^{-\zeta}\big)\big(E_{n+1}^\zeta - E_{n+1}^{-\zeta}\big)\big(E_n^\zeta E_{n+1}^{\zeta}\big)\big(E_{n+1}^\zeta - E_n^{\zeta}\big)} \times\left(\frac{1}{\xi+E_n^\zeta - E_{n+1}^{\zeta}}+\frac{1}{\xi - E_n^\zeta + E_{n+1}^{\zeta}}\right)\big[n_{\rm F}(E_{n}^{\zeta}) - n_{\rm F}(E_{n+1}^{\zeta})\big], \tag{C1c}$$

Similar calculations leads to the Hall conductivity given by Eq. (17) in which the different terms are

$$\sigma^{K,\zeta}_{xy,f-c}(\omega)=\frac{e^2}{h}\sum_{n=0}^{\infty}\frac{\beta_2^2-\beta_1^2+\frac{n\beta_2^4}{E^+_{n-1}E^-_{n-1}}-\frac{(n+1)\beta_1^4}{E^+_{n+1}E^-_{n+1}}}{E_n^{\zeta}-E_n^{-\zeta}}\left(\frac{1}{\xi-E_n^{\zeta}}-\frac{1}{\xi+E_n^{\zeta}}\right)\left[n_{\mathrm{F}}(0)-n_{\mathrm{F}}\left(E_n^{\zeta}\right)\right], \tag{C2a}$$

$$\sigma^{K,\zeta}_{xy,c-c,\mathrm{inter}}(\omega)=\frac{e^2}{h}\sum_{n=0}^{\infty}\frac{(n+1)\left(\beta_1^2E_n^{\zeta}+\beta_2^2E_{n+1}^{-\zeta}\right)^2}{\left(E_n^{\zeta}-E_n^{-\zeta}\right)\left(E_{n+1}^{\zeta}-E_{n+1}^{-\zeta}\right)\left(-E_n^{\zeta}E_{n+1}^{-\zeta}\right)\left(E_n^{\zeta}-E_{n+1}^{-\zeta}\right)}$$
$$\times\left(\frac{1}{\xi+E_n^{\zeta}-E_{n+1}^{-\zeta}}-\frac{1}{\xi-E_n^{\zeta}+E_{n+1}^{-\zeta}}\right)\left[n_{\mathrm{F}}\left(E_{n+1}^{-\zeta}\right)-n_{\mathrm{F}}\left(E_n^{\zeta}\right)\right], \tag{C2b}$$

$$\sigma^{K,\zeta}_{xy,c-c,\mathrm{intra}}(\omega)=\frac{e^2}{h}\sum_{n=0}^{\infty}\frac{(n+1)\left(\beta_1^2E_n^{\zeta}+\beta_2^2E_{n+1}^{\zeta}\right)^2}{\left(E_n^{\zeta}-E_n^{-\zeta}\right)\left(E_{n+1}^{\zeta}-E_{n+1}^{-\zeta}\right)\left(E_n^{\zeta}E_{n+1}^{\zeta}\right)\left(E_{n+1}^{\zeta}-E_n^{\zeta}\right)}$$
$$\times\left(\frac{1}{\xi+E_n^{\zeta}-E_{n+1}^{\zeta}}-\frac{1}{\xi-E_n^{\zeta}+E_{n+1}^{\zeta}}\right)\left[n_{\mathrm{F}}\left(E_n^{\zeta}\right)-n_{\mathrm{F}}\left(E_{n+1}^{\zeta}\right)\right], \tag{C2c}$$

where $n_{\mathrm{F}}(E)=1/(e^{(E-\mu)/(k_BT)}+1)$ is the Fermi distribution function, μ is the Fermi energy, and $\xi=\hbar\omega+i\eta$.

[1] A. H. Castro Neto, F. Guinea, N. M. R. Peres, K. S. Novoselov, and A. K. Geim, Rev. Mod. Phys. **81**, 109 (2009).

[2] M. Z. Hasan and C. L. Kane, Rev. Mod. Phys. **82**, 3045 (2010).

[3] X.-L. Qi and S.-C. Zhang, Rev. Mod. Phys. **83**, 1057 (2011).

[4] K. S. Novoselov, A. K. Geim, S. V. Morozov, D. Jiang, M. I. Katsnelson, I. V. Grigorieva, S. V. Dubonos, and A. A. Firsov, Nature (London) **438**, 197 (2005).

[5] D. Green, L. Santos, and C. Chamon, Phys. Rev. B **82**, 075104 (2010).

[6] D. F. Urban, D. Bercioux, M. Wimmer, and W. Häusler, Phys. Rev. B **84**, 115136 (2011).

[7] D. Bercioux, D. F. Urban, H. Grabert, and W. Häusler, Phys. Rev. A **80**, 063603 (2009).

[8] Z. Lan, N. Goldman, A. Bermudez, W. Lu, and P. Öhberg, Phys. Rev. B **84**, 165115 (2011).

[9] H. Watanabe, Y. Hatsugai, and H. Aoki, J. Phys.: Conf. Ser. **334**, 012044 (2011).

[10] B. Dóra, J. Kailasvuori, and R. Moessner, Phys. Rev. B **84**, 195422 (2011).

[11] F. Piéchon, J.-N. Fuchs, A. Raoux, and G. Montambaux, J. Phys.: Conf. Ser. **603**, 012001 (2015).

[12] A. Raoux, M. Morigi, J.-N. Fuchs, F. Piéchon, and G. Montambaux, Phys. Rev. Lett. **112**, 026402 (2014).

[13] J. Vidal, R. Mosseri, and B. Douçot, Phys. Rev. Lett. **81**, 5888 (1998).

[14] B. Dóra, I. F. Herbut, and R. Moessner, Phys. Rev. B **90**, 045310 (2014).

[15] E. Illes, J. P. Carbotte, and E. J. Nicol, Phys. Rev. B **92**, 245410 (2015).

[16] S. Mukherjee, A. Spracklen, D. Choudhury, N. Goldman, P. Öhberg, E. Andersson, and R. R. Thomson, Phys. Rev. Lett. **114**, 245504 (2015).

[17] R. A. Vicencio, C. Cantillano, L. Morales-Inostroza, B. Real, C. Mejía-Cortés, S. Weimann, A. Szameit, and M. I. Molina, Phys. Rev. Lett. **114**, 245503 (2015).

[18] D. Guzmán-Silva, C. Mejía-Cortés, M. A. Bandres, M. C. Rechtsman, S. Weimann, S. Nolte, M. Segev, A. Szameit, and R. A. Vicencio, New J. Phys. **16**, 063061 (2014).

[19] V. P. Gusynin and S. G. Sharapov, Phys. Rev. B **73**, 245411 (2006).

[20] V. P. Gusynin, S. G. Sharapov, and J. P. Carbotte, J. Phys.: Condens. Matter **19**, 026222 (2007).

[21] E. V. Gorbar, V. P. Gusynin, A. B. Kuzmenko, and S. G. Sharapov, Phys. Rev. B **86**, 075414 (2012).

[22] A. Chodos, K. Everding, and D. A. Owen, Phys. Rev. D **42**, 2881 (1990).

[23] G. D. Mahan, *Many-Particle Physics*, 2nd ed. (Plenum Press, New York and London, 1990).

[24] T. Biswas and T. K. Ghosh, J. Phys.: Condens. Matter **28**, 495302 (2016).

[25] F. Zhang, *Matrix Theory* (Springer-Verlag, New York, 2011).

[26] R. A. Horn and C. R. Johnson, *Matrix Analysis* (Cambridge University Press, Cambridge, UK, 1985).